Analytic Theory for Dilute Colloids in a Charged Slit

Dirk Gillespie

Department of Molecular Biophysics and Physiology, Rush University Medical Center, Chicago, IL

Received: December 23, 2009; Revised Manuscript Received: February 4, 2010

Nanofluidic devices can now be manufactured with a slit-like geometry whose charged walls are 50−1000 nm wide. Through these slits, large charged macromolecules at very low concentration suspended in electrolytes can flow and be analyzed and separated based on their charge and other properties. To study such a system and to compute the flow of these colloidal macromolecules, the equilibrium distribution across the slit (perpendicular to the flow) is needed. Here, an analytic theory for such a concentration distribution of dilute colloid particles in a charged slit is presented. The theory is based on classical density functional theory (DFT) of fluids with the colloid particles described as large, charged, hard spheres and the background electrolyte described as point charges. In the limit of a very dilute colloid, low surface charge on the slit walls, and noninteracting electrical double layers at these walls, the approximate theory is quantitatively correct when compared to numerical solutions of the DFT equations. Outside of this regime of parameters, the approximate theory is generally qualitatively correct, especially when the colloid particles and the slit have the same sign charge.

1. Introduction

Colloid particles suspended in electrolytes have been studied for decades. These particles range from 1 nm to 10 μm in diameter and have tens to thousands of charges, so that even though they are very large, they are easily dissolved in an electrolyte. Such colloids have been described with many theories including DLVO theory[1,2] and density functional theory (DFT) of fluids.[3−5] DLVO uses linearized Poisson−Boltzmann theory to describe how the ions of the electrolyte arrange around a colloid particle, while DFT (described below in detail) includes nonlinear correlations between the ions and the colloid particle.

While colloids have been extensively studied, new applications like nanofluidic devices continue to make colloids a valuable field of study. Nanofluidic devices can transport charged particles (including colloid particles) through cylindrical pores and slit-like channels that are ∼5−1000 nm wide.[6−16] Often, the walls of these pores and channels are also charged, so that they can not only distinguish cations from anions but also divalent cations from monovalent cations.[13,17] Moreover, these systems are now being used to separate (macro)molecules at very low concentrations by charge and other properties.[6−16] They are also used to study the fundamental properties of fluids in a nanopore by measuring the distribution and speed of fluorescent dyes (both neutral and charged dyes).[11−13] In all of these applications, large molecules (here, collectively referred to as colloid particles) at very low concentrations flow through these nanofluidic devices in a background of electrolyte buffer.

As a first step to studying the colloids within such systems, the equilibrium profile of the colloid particles is necessary. These give insight into how these particles behave in such an environment as conditions (e.g., colloid and electrolyte concentrations and surface charge on the device walls) change. Moreover, equilibrium density and electrostatic potential profiles across the pore or slit (perpendicular to the direction of flow) are a starting point for approximate theories to compute the flow of these particles down the nanochannel.[12,18−20]

In this paper, an analytic theory for the equilibrium profile of colloid particles is developed for the charged slit. While theories like DFT exist to compute this, the theory developed here has explicit formulas for the result. The hope is that this makes the theory more accessible while at the same time still being very accurate in the low-concentration regime for which it was designed. Moreover, it appears to be the first analytic theory for computing the density profile of colloidal particles developed from DFT of charged hard spheres. DFT has the advantage of being accurate (i.e., it computes the same results as Monte Carlo simulations for the same system[21−25]) because it includes correlations among all particles. However, DFT has the disadvantage of requiring specialized computer programs (which are not generally available) because of the complicated mathematical structure of the theory (described below).

The analytic theory described here is designed for dilute colloids in a charged slit that is wide enough for the two electrical double layers created by the electrolyte ions to be independent. Moreover, the surface charges on the slit walls should be small, and the electrolyte ions should be much smaller in size than the colloid particles. Within this regime, the theory is accurate when compared to the full DFT equations. Outside of this regime, the theory is only qualitative correct.

This paper is outlined as follows. Section 2 describes the derivation of the theory in detail, with subsections describing the calculation of the electrolyte ions and the electrical double layers and the full DFT theory and the limits needed to derive the theory. Section 3 summarizes the final formulas, compares the results to the full DFT calculations to assess the accuracy of the theory, and discusses the importance of the terms that are included in the DFT but not some other theories. The Appendix details some integrals needed for the derivation.

2. Derivation of the Theory

In this paper, the focus is on a very dilute concentration of large, charged colloid particles (subscript CP) and a low-concentration electrolyte (with ion species subscripted i) in a charged slit of width L centered at $x = 0$ ($-L/2 \leq x \leq L/2$). The walls have surface charge σ_1 on the wall at $x = -L/2$ and σ_2 on the wall at $x = L/2$. In this section, an analytic theory is

described to determine the concentration profile of the colloid particles across the slit ($\rho_{CP}(x)$).

This profile can be determined in equilibrium by

$$\rho_{CP}(x) = \rho_{CP}^{bath} \exp\left[-\frac{1}{kT}(\mu_{CP}^{ex}(x) - \mu_{CP}^{ex,bath})\right] \quad (1)$$

where μ^{ex} is the excess chemical potential. In this paper, it is assumed that the colloid particles are infinitely dilute and that each colloid particle is a charged hard sphere with valence z_{CP} and radius R_{CP}. The surrounding electrolyte is modeled as point charges in the electrostatic mean field because they are small compared to both L and R_{CP}. In that case, the excess chemical potential can be decomposed into a hard-sphere (HS) term and an electrostatic (ES) with density functional theory (DFT) of fluids[22]

$$\mu_{CP}^{ex}(x) = \mu_{CP}^{HS}(x) + \mu_{CP}^{ES}(x) \quad (2)$$

Below, both of these terms are approximated with DFT in the limit of $\rho_{CP}(x) \rightarrow 0$ (the colloid particles are infinitely dilute), and the surrounding electrolyte is described with linearized Poisson−Boltzmann (LPB) theory.

2.1. Approximating the Electrolyte. With DFT, one can compute the energy to insert one colloid particle into a background concentration profile of the electrolyte ions in the charged slit $\{\rho_i(x)\}$. To compute these concentration profiles, LPB theory will be used for the electrostatic potential $\phi(x)$—and for the potential only. This use of the LPB is necessary to be able to analytically compute the electrostatic potential profile $\phi(x)$ across the pore. LPB is a mathematical approximation of the nonlinear Poisson−Boltzmann problem. For the potential, this is generally a misdemeanor; the resulting $\phi(x)$ is numerically different from the nonlinear Poisson−Boltzmann problem but qualitatively correct even when outside of the assumptions used to make the linearization, namely, that $\phi(x) \ll kT/e$. For the concentrations, however, the LPB approximation

$$\rho_i(x) = \rho_i^{bath} \exp\left(-\frac{z_i e}{kT}\phi(x)\right) \approx \rho_i^{bath}\left(1 - \frac{z_i e}{kT}\phi(x)\right) \quad (3)$$

can be a felony; the profile $\rho_i(x)$ is qualitatively incorrect when $\phi(x) \gtrsim kT/e$ because at least one of the concentrations becomes negative. To prevent this and to have the largest range of applicability, a series expansion of the nonlinear exponential form (describe below) is used. This approach extends the range of applicability of the theory well beyond the LPB approximation where $\phi(x) \ll kT/e$. In fact, in Figure 2, it will be shown that even for $\phi(x) > kT/e$, this approach still gives accurate results for the colloid distribution.

In the charged slit, $\phi(x)$ is a superposition of two Gouy−Chapman (GC) solutions, one for the wall at $x = -L/2$ with surface charge σ_1 and one for the other wall at $x = L/2$ with surface charge σ_2. Specifically

$$\phi(x) = \phi_{GC}^{\sigma_1}(x) + \phi_{GC}^{\sigma_2}(x) \quad (4)$$

where each component satisfies its own LPB equation

$$-\epsilon\epsilon_0\frac{d^2\phi_{GC}^{\sigma_1}}{dx^2}(x) = -\frac{e^2}{kT}\left(\sum_i z_i^2\rho_i^{bath}\right)\phi_{GC}^{\sigma_1}(x) + \sigma_1\delta\left(x + \frac{L}{2}\right) \quad (5)$$

where δ is the Dirac delta function and the constants are as follows: k is the Boltzmann constant, T the absolute temperature, e the fundamental charge, ϵ the relative dielectric constant of the system, and ϵ_0 the permittivity of free space. At the other wall, $\phi_{GC}^{\sigma_2}(x)$ satisfies a similar equation. Since it is assumed that these walls are far enough apart not to interact so that

$$\phi_{GC}^{\sigma_1}(x) \approx \phi_{GC}^{\sigma_2}(x) \approx 0 \quad (-R_{CP} < x < R_{CP}) \quad (6)$$

these functions are the classic double layer solutions[26]

$$\phi_{GC}^{\sigma_1}(x) = \frac{\sigma_1}{\kappa\epsilon\epsilon_0}\exp\left[-\kappa\left(x + \frac{L}{2}\right)\right] \quad (7)$$

and

$$\phi_{GC}^{\sigma_2}(x) = \frac{\sigma_2}{\kappa\epsilon\epsilon_0}\exp\left[-\kappa\left(\frac{L}{2} - x\right)\right] \quad (8)$$

where κ^{-1} is the Debye length given by

$$\kappa = \sqrt{\frac{e^2}{\epsilon\epsilon_0 kT}\sum_i z_i^2\rho_i^{bath}} \quad (9)$$

For the electrolyte concentration profiles, eq 6 gives

$$\rho_i(x) \approx \begin{cases} \rho_i^{bath}\exp\left(-\frac{z_i e}{kT}\phi_{GC}^{\sigma_1}(x)\right) & \text{if } -\frac{L}{2} < x < 0 \\ \rho_i^{bath}\exp\left(-\frac{z_i e}{kT}\phi_{GC}^{\sigma_2}(x)\right) & \text{if } 0 \leq x < \frac{L}{2} \\ 0 & \text{if } |x| > \frac{L}{2} \end{cases} \quad (10)$$

because the electrolyte concentration is 0 outside of the slit. As described above, the exponential form is retained so that instead of linearizing the exponential in eq 10, the exponential is expanded into the full infinite series

$$\exp\left(-\frac{z_i e}{kT}\phi_{GC}^{\sigma_1}(x)\right) = \sum_{n=0}^{\infty}\frac{(-1)^n}{n!}\left(\frac{z_i e}{kT}\phi_{GC}^{\sigma_1}(x)\right)^n \quad (11)$$

$$= \sum_{n=0}^{\infty}z_i^n\alpha_1^{(n)}\exp\left[-n\kappa\left(x + \frac{L}{2}\right)\right] \quad (12)$$

and similarly

$$\exp\left(-\frac{z_i e}{kT}\phi_{GC}^{\sigma_2}(x)\right) = \sum_{n=0}^{\infty}z_i^n\alpha_2^{(n)}\exp\left[-n\kappa\left(\frac{L}{2} - x\right)\right] \quad (13)$$

where, for $s = 1$ or 2

$$\alpha_s^{(n)} = \frac{(-1)^n}{n!}\left(\frac{e}{kT}\frac{\sigma_s}{\kappa\epsilon\epsilon_0}\right)^n \tag{14}$$

Note that there is a recursion formula for these coefficients so that ratios of powers of large n and $n!$ do not need to be calculated

$$\alpha_s^{(n+1)} = \frac{-1}{n+1}\frac{e}{kT}\frac{\sigma_s}{\kappa\epsilon\epsilon_0}\alpha_s^{(n)} \tag{15}$$

It is possible to estimate how many terms are required to achieve a given accuracy ε because the Gouy−Chapman solutions are monotonic, with maximum values of $\sigma_1/\kappa\epsilon\epsilon_0$ and $\sigma_2/\kappa\epsilon\epsilon_0$. Then, the last term of the series at $x = -L/2$ or $x = L/2$ must be less than ε

$$\varepsilon > \left|\frac{(-1)^n}{n!}\left(\frac{z_ie}{kT}\frac{\sigma}{\kappa\epsilon\epsilon_0}\right)^n\right| \tag{16}$$

$$= \frac{1}{n!}\left|\frac{z_ie}{kT}\frac{\sigma}{\kappa\epsilon\epsilon_0}\right|^n \tag{17}$$

For $|(z_ie/kT)(\sigma/\kappa\epsilon\epsilon_0)| = 2$, $n = 20$ gives an accuracy of $<10^{-12}$. Therefore, a very reasonable number of terms in the expansions gives highly accurate results for the concentrations that will always be qualitivative correct. Moreover, only for $|(z_ie/kT)(\sigma/\kappa\epsilon\epsilon_0)| \leq 0.1$ does the linearized ($n = 1$) approximation for the concentration (eq 3) give an error of less than 10%.

2.2. DFT of Charged Hard Spheres. *2.2.1. Hard-Sphere Component.* The hard-sphere component of the excess chemical potential $\mu_{CP}^{HS}(x)$ (see eq 2) is described with the fundamental measure theory DFT of Rosenfeld,[22,27] where

$$\mu_{CP}^{HS}(x) = kT\sum_\alpha \int_{x-R_{CP}}^{x+R_{CP}} \frac{\partial\Phi_{HS}}{\partial n_\alpha}(x')W_{CP}^{(\alpha)}(x - x')dx' \tag{18}$$

where (with electrolyte ion species subscripted i and the colloid particles CP)

$$n_\alpha(x) = \sum_i \int_{x-R_i}^{x+R_i} \rho_i(x')W_i^{(\alpha)}(x' - x)dx' +$$

$$\int_{x-R_{CP}}^{x+R_{CP}} \rho_{CP}(x')W_{CP}^{(\alpha)}(x' - x)dx' \tag{19}$$

and for the planar geometry of the slit[22]

$$W_k^{(2)}(r) = 2\pi R_k \tag{20}$$

$$W_k^{(3)}(r) = \pi(R_k^2 - r^2) \tag{21}$$

$$W_k^{(V2)}(r) = 2\pi r \tag{22}$$

$$4\pi R_k^2 W_k^{(0)}(r) = 4\pi R_k W_k^{(1)}(r) = W_k^{(2)}(r) \tag{23}$$

$$4\pi R_k W_k^{(V1)}(r) = W_k^{(V2)}(r) \tag{24}$$

Here, the antisymmetrized excess free energy density $\Phi_{HS}(\{n_\alpha(\mathbf{x})\})^{28}$ (eq 27 of ref 28) is used

$$\Phi_{HS}(\{n_\alpha(\mathbf{x})\}) = -n_0\ln(1 - n_3) + \frac{n_1n_2 - n_{V1}n_{V2}}{1 - n_3} +$$

$$\frac{n_2^3}{24\pi(1 - n_3)^2}\left(1 - \frac{n_{V2}n_{V2}}{n_2^2}\right)^3 \tag{25}$$

For dilute colloid particles and small ions, eqs 18 and 19 can be approximated by taking the limits $\rho_{CP}(x) \rightarrow 0$ (to compute the energy required to insert only one colloid particle into the background concentration profiles of the ions) and $R_i \rightarrow 0$ (with $R_{CP} \neq 0$). It is straightforward to show in these limits that only n_0 does not go to 0 with

$$n_0(x) = \sum_i \lim_{R_i\to 0}\frac{\int_{x-R_i}^{x+R_i}\rho_i(x')dx'}{2R_i} = \sum_i \rho_i(x) \tag{26}$$

Also, for the $\partial\Phi_{HS}/\partial n_\alpha$, only $\partial\Phi_{HS}/\partial n_3$ does not go to 0 since

$$\frac{\partial\Phi_{HS}}{\partial n_3} = \frac{n_0}{1 - n_3} + \frac{n_1n_2 - n_{V1}n_{V2}}{(1 - n_3)^2} +$$

$$\frac{n_2^3}{12\pi(1 - n_3)^3}\left(1 - \frac{n_{V2}n_{V2}}{n_2^2}\right)^3 \tag{27}$$

$$\rightarrow n_0 \tag{28}$$

because the $n_\alpha \rightarrow 0$ except for $\alpha = 0$ and because the limits of the fractions in eq 25 also go to 0. Therefore

$$\mu_{CP}^{HS}(x) = kT\pi\int_{x-R_{CP}}^{x+R_{CP}}\left(\sum_i\rho_i(x')\right)(R_{CP}^2 - (x - x')^2)dx' \tag{29}$$

For the bath concentrations, this reduces to

$$\mu_{CP}^{HS,bath} = kT\frac{4\pi}{3}R_{CP}^3\sum_i\rho_i^{bath} \tag{30}$$

By eq 73 in the Appendix

$$\frac{\mu_{CP}^{HS}(x)}{kT} = \pi\sum_{n=0}^{\infty}\left(\sum_i z_i^n\rho_i^{bath}\right)\alpha_s^{(n)}(R_{CP}^2 C_s^{(n)}(x;0) - C_s^{(n)}(x;2)) \tag{31}$$

where $s = 1$ if $x < 0$ and $s = 2$ if $x \geq 0$.

Analytic Theory for Dilute Colloids in a Charged Slit

J. Phys. Chem. B, Vol. 114, No. 12, 2010 **4305**

2.2.2. Electrostatic Component. For the electrostatic component of the excess chemical potential $\mu_{CP}^{ES}(x)$ in eq 2, several DFTs exist. The most common of these expand $\mu_{CP}^{ES}(x)$ around a reference fluid with densities $\{\rho_k^{ref}(x)\}$[22,29]

$$\mu_{CP}^{ES}(x) = \mu_{CP}^{ES}(\{\rho_k^{ref}(x)\}) - z_{CP}e\phi(x) - kT\sum_k \int_{x-R_{CP}}^{x+R_{CP}} \gamma_{CP,k}(x-x')\Delta\rho_k(x')dx' \quad (32)$$

where

$$\Delta\rho_k(x) = \rho_k(x) - \rho_k^{ref}(x) \quad (33)$$

In the planar geometry of the slit with $R_i \to 0$[29]

$$\gamma_{CP,k}(x-x') = A - \Lambda^2|x'-x| + \Lambda(x-x')^2 - \frac{1}{3}|x'-x|^3 \quad (34)$$

where

$$A = \frac{1}{3}R_{CP}^3 - \Lambda R_{CP}^2 + \Lambda^2 R_{CP} \quad (35)$$

and

$$\Lambda = R_{CP} + \frac{2}{\kappa} \quad (36)$$

There are several possibilities for the reference fluid densities. Here, the simplest choice is made, namely, the bath concentrations

$$\rho_k^{ref}(x) = \rho_k^{bath} \quad (37)$$

Another choice is the "reference fluid density" (RFD) functional.[29,30] While this is generally more accurate,[24] the choice of bulk fluid densities is sufficient here, as shown below where the analytical theory is compared with the RFD functional (Figures 1−3).

With these choices

$$\mu_{CP}^{ES}(\{\rho_k^{ref}(x)\}) = \mu_{CP}^{ES,bulk} \quad (38)$$

Then

$$\mu_{CP}^{ES}(x) - \mu_{CP}^{ES,bulk} = z_{CP}e\phi(x) - kT\frac{z_{CP}e^2}{8\epsilon\epsilon_0}\frac{\kappa}{R_{CP}+\frac{1}{\kappa}}M(x) \quad (39)$$

where

$$M(x) = \int_{x-R_{CP}}^{x+R_{CP}}(\sum_i z_i\rho_i(x'))\gamma_{CP,k}(x-x')dx' \quad (40)$$

$$= \sum_{n=0}^{\infty}(\sum_i z_i^{n+1}\rho_i^{bath})\alpha_s^{(n)}D_s^{(n)}(x) \quad (41)$$

where by eq 73

$$D_s^{(n)}(x) = AC_s^{(n)}(x;0) - \Lambda^2 C_s^{(n)}(x;1) + \Lambda C_s^{(n)}(x;2) - \frac{1}{3}C_s^{(n)}(x;3) \quad (42)$$

As before, $s = 1$ if $x < 0$, and $s = 2$ if $x \geq 0$.

3. Discussion

3.1. Summary. The analytical DFT theory derived in the previous section is for a slit over $-L/2 \leq x \leq L/2$ with surface charge σ_1 at $x = -L/2$ and σ_2 at $x = L/2$. It gives the equilibrium density profile of the colloid particle with valence z_{CP} and radius R_{CP} across the slit by

$$\rho_{CP}(x) = \rho_{CP}^{bath}\exp\left[-\frac{1}{kT}(\mu_{CP}^{ex}(x) - \mu_{CP}^{ex,bath})\right] \quad (43)$$

where

$$-\frac{1}{kT}(\mu_{CP}^{ex}(x) - \mu_{CP}^{ex,bath}) = -\frac{\mu_{CP}^{HS}(x)}{kT} + \frac{4\pi}{3}R_{CP}^3\sum_i \rho_i^{bath} - \frac{z_{CP}e}{kT}\phi(x) - \frac{z_{CP}e^2}{8\epsilon\epsilon_0}\frac{\kappa}{R_{CP}+\frac{1}{\kappa}}M(x) \quad (44)$$

Here

$$\phi(x) = \frac{\sigma_1}{\kappa\epsilon\epsilon_0}\exp\left[-\kappa\left(x+\frac{L}{2}\right)\right] + \frac{\sigma_2}{\kappa\epsilon\epsilon_0}\exp\left[-\kappa\left(\frac{L}{2}-x\right)\right] \quad (45)$$

where κ is given by eq 9 and

$$\frac{\mu_{CP}^{HS}(x)}{kT} = \pi\sum_{n=0}^{\infty}(\sum_i z_i^n\rho_i^{bath})\alpha_s^{(n)}(R_{CP}^2C_s^{(n)}(x;0) - C_s^{(n)}(x;2)) \quad (46)$$

where the functions $C_s^{(n)}(x;a)$ are defined in eqs 75 and 78 as well as eqs 63 − 67. The $\alpha_s^{(n)}$ are given by eq 15 with $\alpha_s^{(0)} = 1$

$$M(x) = \sum_{n=0}^{\infty}(\sum_i z_i^{n+1}\rho_i^{bath})\alpha_s^{(n)}D_s^{(n)}(x) \quad (47)$$

where the functions $D_s^{(n)}(x)$ are defined in eq 42 as well as eqs 35 and 36. If $x < 0$, then $s = 1$; if $x \geq 0$, then $s = 2$. The constants are as follows: k is the Boltzmann constant, T the absolute temperature, e the fundamental charge, ϵ the relative dielectric constant of the system, and ϵ_0 the permittivity of free space. The slit is in equilibrium with a bath with ion species i at concentration ρ_i^{bath} and the colloid particles at concentration ρ_{CP}^{bath}.

3.2. Comparison to Full DFT. To show the accuracy of the approximate analytic DFT theory, the equations summarized above are compared against the solutions of the full RFD DFT theory.[29,30] Specifically, a charged slit of width 50 or 100 nm and equal surface σ on each wall is considered. The slit is in
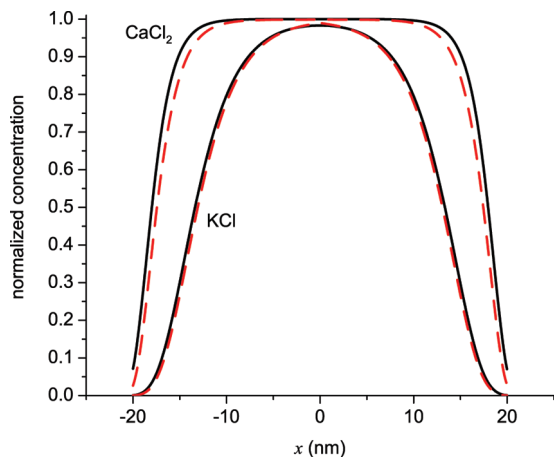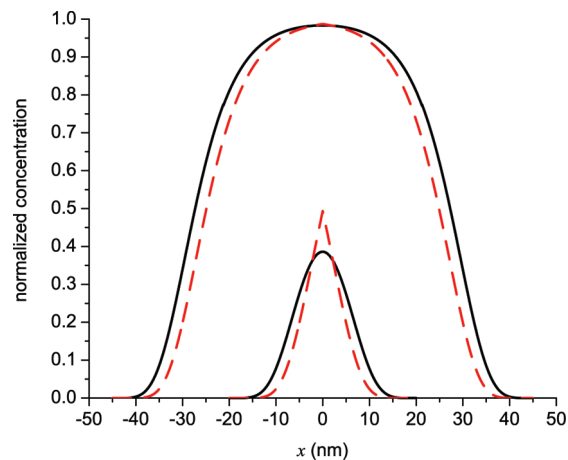
Figure 1. The colloid particle concentration profile across a 50 nm wide slit, normalized to the colloid bath concentration. Both slit walls have $\sigma = -0.01$ C/m^2, and the indicated electrolyte has a bath concentration of 10 mM. The slit is in $-25 \leq x \leq 25$ nm, so that the center of the colloid particle can only reach $-20 \leq x \leq 20$ nm. The solid (black) lines are solutions to the full DFT equations, and the dashed (red) lines are the approximate theory.

Figure 2. The colloid particle concentration profile across a 50 and 100 nm wide slit, normalized to the colloid bath concentration. Both slit walls have $\sigma = -0.01$ C/m^2, and the KCl electrolyte has the bath at 2.5 mM. The solid (black) lines are solutions to the full DFT equations, and the dashed (red) lines are the approximate theory.

equilibrium with a bath containing either KCl or CaCl$_2$ at 2.5 or 10 mM and colloid particles at a 0.01% space filled fraction (i.e., $10^{-4} = 4\pi R_{CP}^3 \rho_{CP}^{bath}/3$), which corresponds to a concentration of $\sim$31.7 nM for $R_{CP} = 5$ nm. Then, a maximum of five particles can fit snugly in a line across the slit; the slit width is on the order of the colloid particle size. The valence of the colloid particle is -10. These are conditions used in many experiments.[6,8,11,13]

In the full DFT calculations, the K$^+$, Ca^{2+}, and Cl$^-$ are given crystal radii of 0.138, 0.100, and 0.181 nm, respectively, while in the approximate theory, they are treated as point particles (when compared to the large colloid particle). This is done to show that the DFT correctly reproduces the point-charge approximation of the electrolyte that is known to be valid for colloid particles and slits of this size. The dielectric constant ϵ of the electrolyte is taken to be 78.4.

Figures 1−3 show that the approximate theory is valid when the electrical double layers at the slit walls do not overlap and when the surface charge on the slit walls is low. This is shown by changing the cation of the electrolyte, the concentration of the electrolyte, and the surface charge σ of the slit walls. Figure 1 shows two cases with $\sigma = -0.01$ C/m^2; the electrolyte is KCl and CaCl$_2$ at 10 mM. When the electrolyte is at 10 mM, in this 50 nm wide slit, the electrical double layers do not interact, and the approximate theory gives excellent results. However, when the two double layers do overlap, the approximate theory becomes only qualitatively correct. This is shown in Figure 2 where the electrolyte is KCl at 2.5 mM in slits that are 50 and 100 nm wide. In the wider slit, the double layers do not overlap, and the approximate solution is still very good, considering that the potential ϕ at the walls is $-1.04kT/e$, which is well outside of the LPB approximation. When the slit is narrower, the double layers overlap, and the approximate solution breaks down. On the basis of these and other numerical experiments (not shown), the approximate theory remains qualitatively correct, in this case showing how the narrower pore admits fewer colloid particles. In general, one can tell in advance that the double layers overlap by checking that eq 6 is valid at $x = 0$ with eqs 7 and 8. Alternatively, one can tell a posteriori when the approximate solution's derivative is not continuous.

Lastly, different slit wall surface charge densities σ are considered. For low colloid particle concentrations (including

at the walls), the approximate theory works well. This is shown in Figure 3 for a slit of width 100 nm to ensure that the electrical double layers do not overlap with the larger surface charge densities. In Figure 3A, the agreement is good for $\sigma = \pm 0.01$ C/m^2 and, in Figure 3B, deteriorates for $\sigma = \pm 0.025$ C/m^2. When the colloid concentration near the wall gets large, the approximate theory does not agree with the full DFT calculations. It is, however, still qualitatively correct.

3.3. Implications for Modeling Nanodevices. The modeling of particles in nanodevices has generally neglected the effect of particle size. However, with current manufacturing techniques, it is possible to create devices that are of comparable size to larger colloid particles. At high concentrations, this can potentially create packing of particles. However, colloid particle size can have significant effects even at the micro- and nanomolar concentrations where fluorescence and other experiments in nanodevices are done.[6,8,11,13]
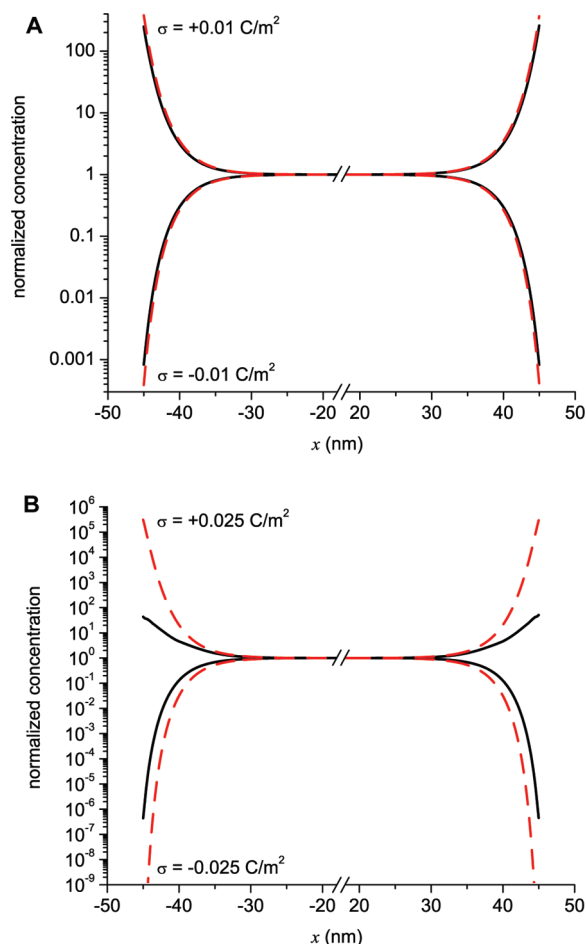
This can be seen by examining the electrochemical potential of the colloid particles (μ_{CP}) in terms of the components described above in eqs 2 and 39

$$\mu_{CP} = kT \ln(\Lambda_{CP}^3 \rho_{CP}(\mathbf{x})) + \mu_{CP}^{HS}(\mathbf{x}) + z_i e\phi(\mathbf{x}) + \mu_{CP}^{SC}(\mathbf{x}) \tag{48}$$

where the screening component[31] μ_{CP}^{SC} (which describes electrostatic correlations beyond the electrostatic mean field ϕ) is the second term on the right-hand side of eq 39. Here, Λ_{CP} is the thermal de Broglie wavelength of the colloid particle and only makes an additive constant to the chemical potential. Figure 4A shows the contribution of the hard-sphere, mean field, and screening terms to the chemical potential for the KCl case of Figure 1A. Specifically, each term is shown with its bath value subtracted. A positive term then reflects an energetic penalty for partitioning from the bath into the slit.

Each component is large, and the hard-sphere and electrostatic terms have a different spatial dependence. The hard-sphere term becomes significant only within a colloid particle radius from the wall. The electrostatic terms, on the other hand, are both approximately equal and become significant approximately within a Debye length of the wall. Both the hard-sphere (excluded volume) and screening terms are set to 0 in the usual Poisson−Boltzmann approach often used in nanopores.[12] Doing

Analytic Theory for Dilute Colloids in a Charged Slit
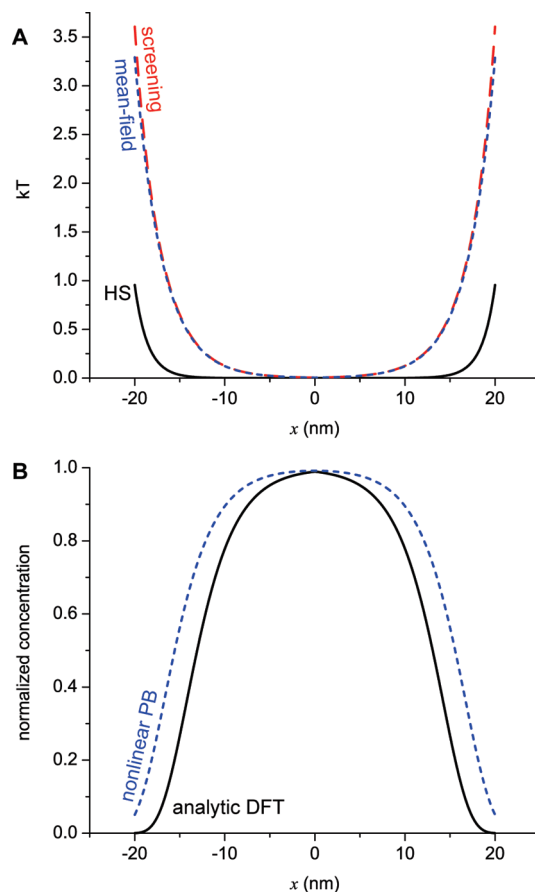
J. Phys. Chem. B, Vol. 114, No. 12, 2010 **4307**

Figure 3. The colloid particle concentration profile across a 100 nm wide slit, normalized to the colloid bath concentration. The KCl electrolyte has a bath of 10 mM. Both slit walls have $\sigma = \pm0.01$ and ±0.025 C/m^2. Because of the width of the slit, the middle 36 nm section is not shown because both the full and approximate solutions have reached the bath concentration. The solid (black) lines are solutions to the full DFT equations, and the dashed (red) lines are the approximate theory.

Figure 4. (A) The components of the excess chemical potential from eq 48 (relative to their bath values) are shown for a 50 nm wide slit with $\sigma = -0.01$ C/m^2 and KCl with a bath concentration of 10 mM (same case as that in Figure 1A). The solid line is the hard-sphere (HS) component, the dashed line is the screening component, and the dotted line is the mean-field component. (B) The solid line is the normalized concentration of the analytical DFT theory from Figure 1A. The dotted line is the numerical solution to the nonlinear Poisson−Boltzmann equations for the colloid particle (i.e., μ_{CP}^{HS} and μ_{CP}^{SC} are both 0). For the Poisson−Boltzmann calculation, the distance of closest approach of the colloid particle was taken to be the particle radius. Both profiles were normalized to the bath concentration.

4. Conclusion

An analytical solution of the DFT equations for charged hard spheres is derived for large, charged (colloid) particles confined in a charged slit while suspended in an electrolyte of ions much smaller than the colloid. This theory was derived with nanofluidic devices in mind, but it is generally applicable to many colloidal systems. The analytic theory is accurate in the limit of an infinitely dilute colloid, low surface charge on the slit walls, and wide enough channel so that the electrical double layers at each slit wall are independent. The results are best when the colloid particles have the same sign of charge as the slit walls. This DFT approach is different from Poisson−Boltzmann theory because the DFT explicitly treats the size of the colloid particles and the correlations that stem from that size, both between the colloid and the ions and the colloid and the slit walls. Therefore, the DFT theory is accurate even when the colloid particles are of the same size as the slit.

Appendix

Mathematical Necessities. To evaluate the DFT equations, several integrals of the $\rho_i(x)$ are needed and are evaluated here.

this produces a different concentration profile for the colloid particles, as shown in Figure 4B. There, the analytic DFT result of Figure 1A is compared to the solution of the full nonlinear Poisson−Boltzmann theory. The DFT solution has the colloid particles more displaced from the wall. Moreover, at the wall, the DFT has zero concentration, while the Poisson−Boltzmann solution has a nonzero concentration.

The size of the screening component is especially noteworthy. Here, it is almost identical to the mean electrostatic potential ϕ. Some theories attempt to include the effect of ion size by including an ad hoc excluded volume term (e.g., ref 32). Such an approach does not, however, include the electrostatic correlations that are in the screening term. For example, in a homogeneous solutions of either NaCl or CaCl$_2$, all of the ions are the same size, and the mean electrostatic potential ϕ is 0. However, the ions will pack around the Ca^{2+} differently than the Na$^+$ because of calcium's +2 charge, producing a different energy for the system. This is captured partly by an excluded volume term but mainly by the screening term, as shown by bulk theories like the mean spherical approximation.[33] In fact, in other systems that have been studied, the screening term can be significantly larger than both the hard-sphere and mean field terms.[25,31]

Specifically, these integrals are

$$\int_{x-R_{CP}}^{x+R_{CP}} \rho_i(x')|x - x'|^k dx' = \int_{x-R_{CP}}^{x} \rho_i(x')(x - x')^k dx' +$$
$$\int_{x}^{x+R_{CP}} \rho_i(x')(x' - x)^k dx' \quad (49)$$

$$= (-1)^{k+1} \int_{x}^{x-R_{CP}} \rho_i(x')(x' - x)^k dx' +$$
$$\int_{x}^{x+R_{CP}} \rho_i(x')(x' - x)^k dx' \quad (50)$$

for $k = 0, 1, 2, 3$. With the expansions in eqs 12 and 13, there are four cases

(1) For $x < 0$,

$$\int_{x}^{x-R_{CP}} \rho_i(x')(x' - x)^k dx' = \rho_i^{bath} \sum_{n=0}^{\infty} z_i^n \alpha_1^{(n)} A_1^{(n)}(x;k)$$
$$(51)$$

where

$$A_1^{(n)}(x;k) = \int_{x}^{X_1} (x' - x)^k \exp\left[-n\kappa\left(x' + \frac{L}{2}\right)\right] dx'$$
$$(52)$$

and

$$X_1 = \max\left\{-\frac{L}{2}, x - R_{CP}\right\} \quad (53)$$

(2) For $x > 0$,

$$\int_{x}^{x-R_{CP}} \rho_i(x')(x' - x)^k dx' = \rho_i^{bath} \sum_{n=0}^{\infty} z_i^n \alpha_2^{(n)} A_2^{(n)}(x;k)$$
$$(54)$$

where

$$A_2^{(n)}(x;k) = \int_{x}^{x-R_{CP}} (x' - x)^k \exp\left[-n\kappa\left(\frac{L}{2} - x'\right)\right] dx'$$
$$(55)$$

(3) For $x < 0$,

$$\int_{x}^{x+R_{CP}} \rho_i(x')(x' - x)^k dx' = \rho_i^{bath} \sum_{n=0}^{\infty} z_i^n \alpha_1^{(n)} B_1^{(n)}(x;k)$$
$$(56)$$

where

$$B_1^{(n)}(x;k) = \int_{x}^{x+R_{CP}} (x' - x)^k \exp\left[-n\kappa\left(x' + \frac{L}{2}\right)\right] dx'$$
$$(57)$$

(4) For $x > 0$,

$$\int_{x}^{x+R_{CP}} \rho_i(x')(x' - x)^k dx' = \rho_i^{bath} \sum_{n=0}^{\infty} z_i^n \alpha_2^{(n)} B_2^{(n)}(x;k)$$
$$(58)$$

where

$$B_2^{(n)}(x;k) = \int_{x}^{X_2} (x' - x)^k \exp\left[-n\kappa\left(\frac{L}{2} - x'\right)\right] dx' \quad (59)$$

and

$$X_2 = \min\left\{\frac{L}{2}, x + R_{CP}\right\} \quad (60)$$

These integrals can be evaluated with the following relationship[34]

$$\int (x' - x)^k e^{ax'+b} dx' = e^{ax+b} \int u^k e^{au} du \quad (61)$$
$$= e^{ax'+b} P_k(x' - x; a) \quad (62)$$

where, for $a \neq 0$

$$P_0(\xi, a) = \frac{1}{a} \quad (63)$$

$$P_1(\xi, a) = \frac{1}{a}\left(\xi - \frac{1}{a}\right) \quad (64)$$

$$P_2(\xi, a) = \frac{1}{a}\left(\xi^2 - \frac{2}{a}\xi + \frac{2}{a^2}\right) \quad (65)$$

$$P_3(\xi, a) = \frac{1}{a}\left(\xi^3 - \frac{3}{a}\xi^2 + \frac{6}{a^2}\xi - \frac{6}{a^3}\right) \quad (66)$$

and, if $a = 0$

$$P_k(\xi, 0) = \frac{1}{k+1}\xi^{k+1} \quad (67)$$

Then

$$A_1^{(n)}(x;k) = \exp\left[-n\kappa\left(X_1 + \frac{L}{2}\right)\right] P_k(X_1 - x, -n\kappa) -$$
$$\exp\left[-n\kappa\left(x + \frac{L}{2}\right)\right] P_k(0, -n\kappa) \quad (68)$$

$$A_2^{(n)}(x;k) = \exp\left[-n\kappa\left(\frac{L}{2} - (x - R_{CP})\right)\right] P_k(-R_{CP}, n\kappa) -$$
$$\exp\left[-n\kappa\left(\frac{L}{2} - x\right)\right] P_k(0, n\kappa) \quad (69)$$

$$B_1^{(n)}(x;k) = \exp\left[-n\kappa\left(x + R_{CP} + \frac{L}{2}\right)\right] P_k(R_{CP}, -n\kappa) -$$
$$\exp\left[-n\kappa\left(x + \frac{L}{2}\right)\right] P_k(0, -n\kappa) \quad (70)$$

$$B_2^{(n)}(x;k) = \exp\left[-n\kappa\left(\frac{L}{2} - X_2\right)\right] P_k(X_2 - x, n\kappa) \quad (71)$$
$$-\exp\left[-n\kappa\left(\frac{L}{2} - x\right)\right] P_k(0, n\kappa) \quad (72)$$

Analytic Theory for Dilute Colloids in a Charged Slit

J. Phys. Chem. B, Vol. 114, No. 12, 2010 **4309**

Therefore, for $x < 0$

$$\int_{x-R_{CP}}^{x+R_{CP}} \rho_i(x')|x - x'|^k dx' = \rho_i^{bath} \sum_{n=0}^{\infty} z_i^n \alpha_1^{(n)} C_1^{(n)}(x;k) \tag{73}$$

where

$$C_1^{(n)}(x;k) = (-1)^{k+1} A_1^{(n)}(x;k) + B_1^{(n)}(x;k) \tag{74}$$

$$= (-1)^{k+1} \exp\left[-n\kappa\left(X_1 + \frac{L}{2}\right)\right] P_k(X_1 - x, -n\kappa) +$$
$$\exp\left[-n\kappa\left(x + R_{CP} + \frac{L}{2}\right)\right] P_k(R_{CP}, -n\kappa) -$$
$$(1 + (-1)^{k+1}) \exp\left[-n\kappa\left(x + \frac{L}{2}\right)\right] P_k(0, -n\kappa) \tag{75}$$

For $x > 0$

$$\int_{x-R_{CP}}^{x+R_{CP}} \rho_i(x')|x - x'|^k dx' = \rho_i^{bath} \sum_{n=0}^{\infty} z_i^n \alpha_2^{(n)} C_2^{(n)}(x;k) \tag{76}$$

where

$$C_2^{(n)}(x;k) = (-1)^{k+1} A_2^{(n)}(x;k) + B_2^{(n)}(x;k) \tag{77}$$

$$= (-1)^{k+1} \exp\left[-n\kappa\left(\frac{L}{2} - (x - R_{CP})\right)\right] \times$$
$$P_k(-R_{CP}, n\kappa) + \exp\left[-n\kappa\left(\frac{L}{2} - X_2\right)\right] P_k(X_2 - x, n\kappa) -$$
$$(1 + (-1)^{k+1}) \exp\left[-n\kappa\left(\frac{L}{2} - x\right)\right] P_k(0, n\kappa) \tag{78}$$

References and Notes

(1) Derjaguin, B.; Landau, L. *Acta Physicochim. URSS* **1941**, *14*, 633–662.

(2) Verwey, E. J.; Overbeek, J. T. G. *Theory of the Stability of Lyophobic Colloids*; Elsevier: Amsterdam, The Netherlands, 1948.

(3) Bechinger, C.; Rudhardt, D.; Leiderer, P.; Roth, R.; Dietrich, S. *Phys. Rev. Lett.* **1999**, *83*, 3960.

(4) Louis, A. A.; Allahyarov, E.; Löwen, H.; Roth, R. *Phys. Rev. E* **2002**, *65*, 061407.

(5) Baumgartl, J.; Dullens, R. P. A.; Dijkstra, M.; Roth, R.; Bechinger, C. *Phys. Rev. Lett.* **2007**, *98*, 198303–4.

(6) Bayley, H.; Martin, C. R. *Chem. Rev.* **2000**, *100*, 2575–2594.

(7) Saleh, O. A.; Sohn, L. L. *Rev. Sci. Instrum.* **2001**, *72*, 4449–4451.

(8) Saleh, O. A.; Sohn, L. L. *Proc. Natl. Acad. Sci. U.S.A.* **2003**, *100*, 820–824.

(9) Ito, T.; Sun, L.; Crooks, R. M. *Anal. Chem.* **2003**, *75*, 2399–2406.

(10) Howorka, S.; Siwy, Z. *Chem. Soc. Rev.* **2009**, *39*, 2360–2384.

(11) Pu, Q.; Yun, J.; Temkin, H.; Liu, S. *Nano Lett.* **2004**, *4*, 1099–1103.

(12) Pennathur, S.; Santiago, J. G. *Anal. Chem.* **2005**, *77*, 6772–6781.

(13) Pennathur, S.; Santiago, J. G. *Anal. Chem.* **2005**, *77*, 6782–6789.

(14) Pennathur, S.; Baldessari, F.; Santiago, J. G.; Kattah, M. G.; Steinman, J. B.; Utz, P. J. *Anal. Chem.* **2007**, *79*, 8316–8322.

(15) Das, S.; Chakraborty, S. *Langmuir* **2008**, *24*, 7704–7710.

(16) Kovarik, M. L.; Jacobson, S. C. *Anal. Chem.* **2009**, *81*, 7133–7140.

(17) Gillespie, D.; Boda, D.; He, Y.; Apel, P.; Siwy, Z. S. *Biophys. J.* **2008**, *95*, 609–619.

(18) Cervera, J.; Schiedt, B.; Ramírez, P. *Europhys. Lett.* **2005**, *71*, 35–41.

(19) Cervera, J.; Schiedt, B.; Neumann, R.; Mafe, S.; Ramirez, P. *J. Chem. Phys.* **2006**, *124*, 104706.

(20) Vlassiouk, I.; Smirnov, S.; Siwy, Z. *Nano Lett.* **2008**, *8*, 1978–1985.

(21) Kierlik, E.; Rosinberg, M. L. *Phys. Rev. A* **1991**, *44*, 5025–5037.

(22) Rosenfeld, Y. *J. Chem. Phys.* **1993**, *98*, 8126–8148.

(23) Roth, R.; Evans, R.; Lang, A.; Kahl, G. *J. Phys.: Condens. Matter* **2002**, *14*, 12063–12078.

(24) Gillespie, D.; Valiskó, M.; Boda, D. *J. Phys.: Condens. Matter* **2005**, *17*, 6609–6626.

(25) Valiskó, M.; Boda, D.; Gillespie, D. *J. Phys. Chem. C* **2007**, *111*, 15575–15585.

(26) Newman, J.; Thomas-Alyea, K. E. *Electrochemical Systems*, 3rd ed.; Wiley-Interscience: Hoboken, NJ, 2004.

(27) Rosenfeld, Y. *Phys. Rev. Lett.* **1989**, *63*, 980–983.

(28) Rosenfeld, Y.; Schmidt, M.; Löwen, H.; Tarazona, P. *Phys. Rev. E* **1997**, *55*, 4245–4263.

(29) Gillespie, D.; Nonner, W.; Eisenberg, R. S. *J. Phys.: Condens. Matter* **2002**, *14*, 12129–12145.

(30) Gillespie, D.; Nonner, W.; Eisenberg, R. S. *Phys. Rev. E* **2003**, *68*, 031503.

(31) Gillespie, D. *Biophys. J.* **2008**, *94*, 1169–1184.

(32) Kilic, M. S.; Bazant, M. Z.; Ajdari, A. *Phys. Rev. E* **2007**, *75*, 021502.

(33) Blum, L. *J. Stat. Phys.* **1980**, *22*, 661–672.

(34) Gradshteyn, I. S.; Ryzhik, I. M. *Table of Integrals, Series, and Products*; Academic Press: San Diego, CA, 2000.